Journal Pre-proof

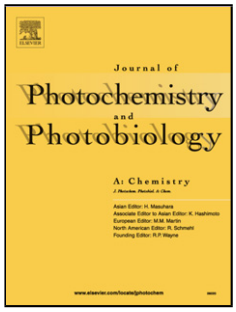

Oxidation of styrene oxide via chemical and photochemical methods using TiO_2-CeO_2-V_2O_5 catalysts

Ma. Elena Manríquez (Conceptualization) (Investigation) (Resources), Martín Trejo Valdez (Formal analysis), Andrea Sánchez Pliego (Methodology), Laura V. Castro (Formal analysis), Emma Ortiz-Islas (Writing - original draft) (Supervision) (Writing - review and editing)

PII: S1010-6030(20)30304-X

DOI: https://doi.org/10.1016/j.jphotochem.2020.112505

Reference: JPC 112505

To appear in: *Journal of Photochemistry & Photobiology, A: Chemistry*

Received Date: 3 December 2019

Revised Date: 6 February 2020

Accepted Date: 15 March 2020

Please cite this article as: Manríquez ME, Valdez MT, Pliego AS, Castro LV, Ortiz-Islas E, Oxidation of styrene oxide via chemical and photochemical methods using TiO_2-CeO_2-V_2O_5 catalysts, *Journal of Photochemistry and amp; Photobiology, A: Chemistry* (2020), doi: https://doi.org/10.1016/j.jphotochem.2020.112505

Oxidation of styrene oxide via chemical and photochemical methods using TiO_2-CeO_2-V_2O_5 catalysts

Ma. Elena Manríquez[a], Martín Trejo Valdez[a], Andrea Sánchez Pliego[1], Laura V. Castro[a], Emma Ortiz-Islas[b*]

[a]Instituto Politécnico Nacional, ESIQIE, Col. Zacatenco, 07738 Ciudad de México, México

[b]Instituto Nacional de Neurología y Neurocirugía, Laboratorio de Nanotecnología, Col. La Fama, 14269 Ciudad de México, México

*Corresponding author: emma170@hotmail.com

Graphical abstract

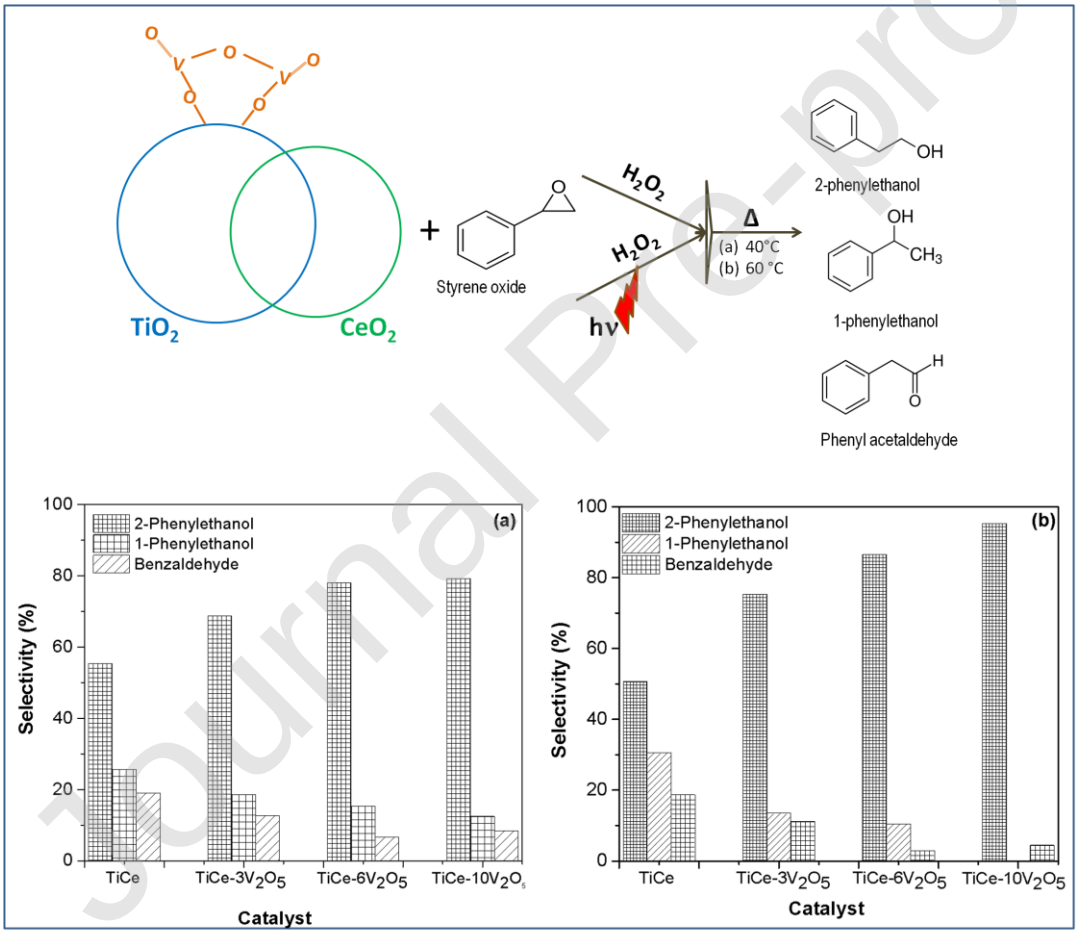

Highlights

- TiO_2-CeO_2/V_2O_5 catalysts were obtained by co-precipitation from individual oxides.
- The catalysts were tested in the oxidation of styrene oxide via photochemical process
- The reaction also took place without light application
- Higher catalytic conversion was obtained when ultraviolet light was applied
- The most considerable selectivity to 2-phenyl ethanol was obtained with light irradiation

Abstract

This work reports the preparation of the TiO_2-CeO_2 (TiCe) catalytic support of V_2O_5 catalysts, which was tested in the oxidation process of styrene oxide via chemical and photochemical methods. The TiCe-V_2O_5 catalytic support was prepared by the co-precipitated method from the individual metal oxides, varying the amount of vanadium oxide by 3, 6, and 10 % mol with respect to the support. The obtained catalysts were characterized by different spectroscopies, as well as by the N_2 adsorption-desorption technique. The catalytic reaction test was carried out in the liquid phase during 120 min with/without ultraviolet light irradiation at 50 ^oC. There was no V_2O_5 effect on the surface area, pore volume, and pore diameter since all catalysts had similar textural values. In all samples the structures identified by X-ray diffraction were the Anatase phase and CeO_2 in the cubic phase. XPS results revealed the formation of surface carbonate species, which were also identified by infrared spectroscopy. The conversion rate was better when employing ultraviolet light, and the rate increased as the V_2O_5 amount rose. The main reaction products were 2-phenylethanol and 1-phenylethanol. However, a low amount of benzaldehyde was detected. The selectivity to the desirable product (2-phenylethanol) increased when the reaction was irradiated with UV light and the catalyst contained a higher amount of vanadium . It was observed that the effect of UV radiation on the electric mobility produces an acceleration of the reaction to 2-phenylethanol, avoiding the 1-phenylethanol formation. The bandgap value decreased as the vanadium oxide amount increased, boosting the electric mobility.

Keywords. Styrene oxide; Photochemical; Chemical; Catalysts; Oxidation.

1. Introduction

The heterogeneous photocatalysis applied to the chemical transformations in a liquid phase is a relatively novel technology for the synthesis of chemical products by selective oxidation [1-3]. Selective photo-oxidation is a new method to obtain partially oxidized organic molecules such as hydrocarbons and alcohols, aldehyde derivatives with full industrial chemical applications (flavor, confectionery, beverages, among others), and epoxies to be used in chemical and plastic industries [3-5]. In recent years selective photocatalytic processes have drawn researchers´ attention to changing from harmful to friendly and sustainable methods. Thus, it is of great importance to have the adequate reaction conditions, for which reason catalysts must have satisfactory oxidizing properties, and be capable in turn of absorbing UV-Vis light. For this work, CeO_2 was selected as part of the catalytic support due to its stability, selectivity, and activity in various photocatalytic applications [6-8]. Several researchers have used the oxygen storage capacity of CeO_2 and its ability to increase the catalytic activity and to reduce coke formation [9-12]. The oxygen storage capacity can be defined as a local source to store or release oxygen; in the reversible redox reaction of $Ce^{3+} \leftrightarrow Ce^{4+}$, in which oxygen is released and reacts with other reagents, the role of cerium has been investigated. Also, the storage capacity of oxygen makes it suitable for use in the oxidation of CO to CO_2 [13,14].

On the other hand, when TiO_2 absorbs a photon of energy greater than or equal to its bandgap (hv≥Eg) it generates the promotion of an electron from the valence band (VB) to the conduction band (CB) promoting the formation of an electron-hole pair ($e^{-}CB$-$h^{+}VB$). These charge carriers can migrate to the catalyst surface to produce oxidation processes [15]. The photogenerated electrons could react with an electron acceptor such as O_2 to form a radical anion O_2•-. While the hole can initiate further interfacial electron transfer or other chemical reactions, it can itself diffuse into the bulk solvent with surface-bound OH- ions. The photogenerated electron (e^{-}) is usually in the conduction band edge, and the hole (h^{+}) is in the valence band edge. The catalyst deactivation by the electron-hole recombination may be difficult if there is a mismatch of energies of electron and hole. Unlike metals, semiconductors lack a continuum of inter-band states to assist the recombination of electron-hole pairs. This fact assures an electron-hole pair lifetime sufficiently long to allow these species to participate in interfacial electron transfer.

Vanadium quickly changes its oxidation state, and it is stable as V^{2+}, V^{3+}, V^{4+} and V^{5+}. Therefore, it is an active catalyst, mainly in oxidation reactions due to the fact that it easily forms oxygen vacancies, adsorbs ultraviolet light, and is capable of creating reactive species such as O_2•- and OH• radicals [16]. The V^{5+} state found in tetrahedral (VO_4), pentahedral (VO_5), and octahedral (VO_6) forms tends to form poli-oxoanions. Surface V^{5+} sites are commonly present as isolated monomeric species from VO_4; in all these forms, vanadium can function as an excellent catalyst [17].

CeO_2-TiO_2-V_2O_5 catalysts have been used to control the emission of highly harmful substances. The simultaneous removal of mercury and nitrogen oxide from a flue gas, by selective catalytic reduction or under oxidation conditions, has been reported [18]. The 1%V_2O_5-10% CeO_2/TiO_2 catalyst showed the best removal efficiency of both mercury and NO; the efficiency was just over 80% at a temperature of 250 °C. In a recent work, it was reported that the CeO_2 loaded on a V_2O_5-TiO_2 support not only did it notably enhance selective catalytic reduction but it also enhanced Hg^0 oxidation [19]. Recently, a V_2O_5-CeO_2-TiO_2-SO_4^{2-} catalyst was tested in the selective catalytic reduction of nitrogen oxide by NH_3 [20]. In this case, V_2O_5-TiO_2 was the catalytic support which showed a low conversion of NO. However, the CeO_2 addition enhanced the NO conversion in a 220-400 °C temperature interval. The sulfated catalyst showed a better conversion rate in comparison with the commercial catalyst.

There is little literature on styrene oxide oxidation, and nothing yet regarding heterogeneous catalysts. Therefore, we are reporting in this paper the application of these catalysts in photocatalytic oxidation, compared to the reaction without light irradiation. The three oxides that make up our catalysts are semiconductors containing V_2O_5 dispersed on mixed CeO_2/TiO_2 supports, with a higher redox potential that promotes defect formation and oxygen transport within the catalyst lattice. Among the objectives of the research was to emphasize the importance of testing catalysts in the oxidation reaction of styrene oxide through the photochemical and chemical pathways, and to correlate the activity of catalysts to the band energy and the effect of the V_2O_5 amount addition.

2. Experimental

2.1 Catalysts preparation

2.1.1 Chemical substances

Ammonium metavanadate (NH_4VO_3) (Sigma-Aldrich, 98 %)

Cerium chloride III heptahydrate ($CeCl_2.7H_2O$) (Sigma-Aldrich, 99 %)

Sodium hydroxide (NaOH) (Sigma-Aldrich, 98 %)

Absolute ethanol (Sigma-Aldrich, 9 7%)

Styrene oxide (Sigma-Aldrich, 97 %)

Hydrogen peroxide solution (Sigma-Aldrich, 30 % (w/w) in H_2O).

TiO_2 (P25-Degussa, Sigma-Aldrich, 98 %)

2.1.2 Procedures

We used the co-precipitation method for the synthesis of the catalysts from alkaline solutions of each precursor using a 1 M sodium hydroxide solution. Table 1 shows the amounts of the chemical substances used for the synthesis of the catalysts. The necessary quantities of V_2O_5 and CeO_2 were calculated considering 5 g of TiO_2 as 100 % and corresponding to 0.062 mol. The CeO_2 amount was constant in all catalysts, and it corresponds to 10 mol %. The mol percentage of V_2O_5 was 3 %, 6 %, and 10 %, respectively.

TiO_2-CeO_2 (TiCe). In addition, an aqueous solution of TiO_2 and $CeCl_2.7H_2O$ was made. Both solutions were mixed, and a solution of NaOH (1 M) was added; then the mixture was heated at 70 °C for 2 h. Subsequently, the obtained precipitate was washed with water and dried at 70 ° C for 5 h. Finally, the catalysts was annealed at 400 °C for 4 h in an air flux.

TiO_2-CeO_2-XV_2O_5 (TiCe-XV_2O_5) X= 3, 6, 10 %. Each of the oxides was prepared by mixing aqueous solutions of $CeCl_2.7H_2O$, TiO_2, with NH_4VO_3 and adding a solution of NaOH (1M) as a precipitating agent. The co-precipitation was performed at pH=10. The solid precipitates were filtered and washed with deionized water, and then dried at 80 °C in air for 12 h. The dried samples were annealed at 400 ºC for 4 h in an air flux.

Table 1. Amounts used of the precursor of titanium, cerium and vanadium oxides.

Sample	TiO_2 (g)	$CeCl_3.7H_2O$ (g)	(NH_4VO_3) (g)
TiCe	5	2.297	0

TiCe-3V_2O_5	5	2.297	0.72
TiCe-6V_2O_5	5	2.297	1.08
TiCe-10V_2O_5	5	2.297	2.2

2.2 Catalysts Characterization

The specific surface area, average pore diameter, and pore volume were determined from the N_2 adsorption-desorption isotherms. The samples were previously thermally treated at 80 °C under vacuum during 12 h. The N_2 gas adsorption-desorption was carried out at 77.3 K using a Belsorp II equipment. The specific surface areas were determined using the Brunauer-Emmet-Teller (BET) method, and the average pore size and pore volume values were determined from the desorption isotherm using the Barret-Joyner-Halenda (BJH) method. The FTIR spectra of all samples were acquired in an Affinity IR spectrometer equipped with an attenuated reflection (Shimadzu) module. All spectra were collected with an average of 100 measurements, a resolution of 8 cm^{-1} and an interval of 1400 to 400 cm^{-1}. Raman spectroscopy was performed in a micro-Raman spectrometer (JobinYvonHR800 model) at room temperature. Line laser excitation was 532 nm with a D3filter and an exposure time of 2 s. The sample powder was placed on a clean glass sample holder and the spectra were recorded in a wavenumber range from 100 cm^{-1} to 1100 cm^{-1}. A THERMO Scientific K-Alpha spectrometer with an Al K X-ray source (1486.6 eV) and a hemispherical electron analyzer was used to determine the surface chemical composition and the valence band of the V_2O_5/CeO_2-TiO_2 catalysts. Experimental peaks were deconvoluted into their components using mixed Gaussian-Lorentzian functions and a non-linear square fitting algorithm, then the Shirley background subtraction was applied. The d-band centers were determined by the integrate of the first moment of the density of state equation 1 by XPS measurements [21].

$$\mu_p = \int N(\varepsilon)\, \varepsilon^p \mathrm{d}\varepsilon \quad (1)$$

Where μp is the moment order, and $N(\varepsilon)$ is the DOS. Thus, d-band centers correspond to the gravity center when $\mu_1/\mu_0 = 1$, and it was integrated from the Fermi level energy to the d-band center energy.

2.3 Catalysts evaluation of the styrene oxide oxidation

2.3.1 Chemical method

The catalytic reaction was carried out in liquid phase, using 1 g of catalyst, 150 ml of absolute ethanol, 2 mmol of styrene oxide, 0.067 mol of H_2O_2 and magnetic stirring. The reaction was carried out at 50 ° C for 2 h.

The products were analyzed and quantified in a Varian Star 3600 CX gas chromatography with capillary column AT-1 of 30 m X 0.25 mm i.D. X 25 μm film.

2.3.2 Photochemical method

The catalytic photoreaction was also carried out in liquid phase, mixing 1 g of catalyst, 150 ml of absolute ethanol, 2 mmol of styrene oxide, and 0.067 mol of H_2O_2 with magnetic stirring and irradiation during 2 h at 50 °C. A UVP Pen-Ray 90-0012-01 11SC-1 Mercury - UV Lamp (254 nm, 2.12 inches, illuminated length) was used, and water was recirculated to the lamp in order to keep its temperature constant at 20 °C and prevent overheating.

The products were analyzed and quantified in a Varian Star 3600 CX gas chromatography with capillary column AT-1 of 30 m X 0.25 mm i.D. X 25 μm film.

2.3.3 Determination of catalytic test parameters

The catalytic conversion, the catalytic selectivity, and the reaction yield were determined from the obtained data of the gas chromatographic analysis and using the following criteria:

- The conversion degree (Xa) is defined as the ratio between the area under the curve of transformed moles and the area under the curve of mole fed for a given compound:

$$Xa = \frac{\mathrm{AP0} - \mathrm{APT}}{\mathrm{AP0}}$$

Where A_{P0} is the area under the curve of the Styrene Oxide mole fed and the A_{PT} is the area under the curve of the transformed Styrene Oxide mole.

- The selectivity (S) of a reaction to a given product (x) is represented by the ratio of the area under the curve of moles of the obtained product between the area under the curve of the mole of all the transformed products (x, y, z, etc.). So:

$$Sx = \frac{\mathrm{APx}}{\mathrm{APx} + \mathrm{APy} + \mathrm{APz}}$$

- The yield of a reaction, concerning some of its products, is calculated by the ratio of the area under the curve of mole of product x obtained (Apx) between the area under the curve of the reactant moles fed:

$$Rx = \frac{\mathrm{APx}}{\mathrm{AP0}}$$

3. Results and discussion

3.1 Nitrogen adsorption-desorption

The N_2 adsorption-desorption isotherms of all catalysts fall within the IUPAC classification in a type III isotherm (Figure 1). All isotherms show a more significant amount of adsorption pressure region (P/P0 > 0.6), and a full hysteresis loop indicating the presence of large mesopores. This assumption is corroborated by the average pore diameter values, which vary between 17 and 19.38 nm (Table 2).

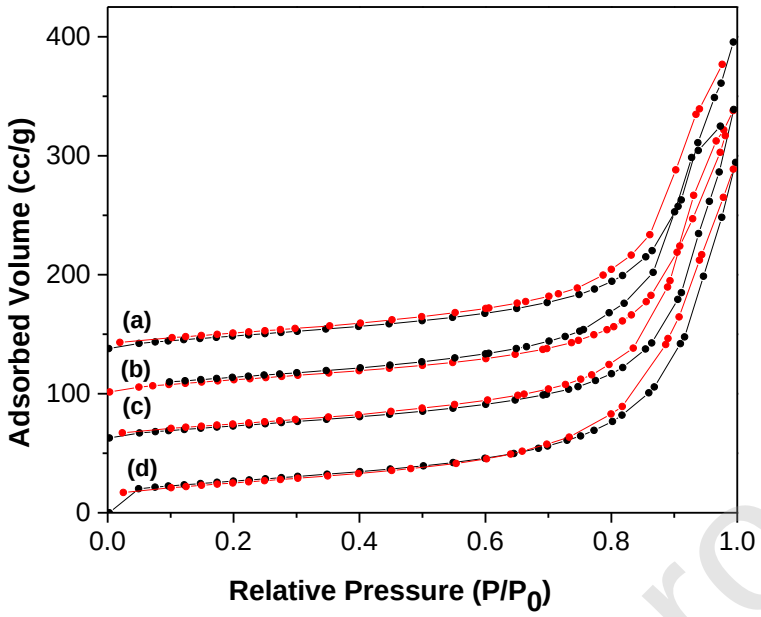

Figure 1. Adsorption (black)-desorption(red) isotherms of (a) TiCe-10V_2O_5, (b) TiCe-6V_2O_5, (c) TiCe-3V_2O_5, and (d) TiCe catalysts.

The Brunauer-Emmett-Teller (BET) surface area of the porous TiCe catalyst was found to be 94 m^2/g, and this area decreased slightly with the addition of vanadium oxide. Using the BJH method and the desorption branch of the nitrogen isotherm, the calculated pore-size distribution data indicated that the TiCe catalyst had an average pore size of 18.4 nm, while the average pore size of catalysts containing V_2O_5 also decreased a little (Table 2). Therefore we can say there is a substantial effect of the V_2O_5 addition on the textural properties since the values shown in Table 2 are very close.

Table 2. Brunauer-Emmett-Teller surface area (S_{BET}), pore diameter (D_P), and pore volume (V_P) of the TiCe and the different TiCe-V_2O_5 catalysts.

Sample	S_{BET} (m^2/g)	D_P (nm)	V_P (cc/g)
TiCe	94	18.4	0.4310
TiCe-3V_2O_5	90	17.026	0.3830

TiCe-6V_2O_5	91	17.732	0.4119
TiCe-10V_2O_5	89	19.385	0.4348

3.2 Infrared spectroscopy

Figure 2 shows the FTIR spectra of TiCe-V_2O_5 catalysts in the wavenumber interval of 1400-400 cm^{-1}. A broad and incomplete band was observed around 420 cm^{-1}, which belongs to the Ti-O-Ti stretching vibrations from structural bonds in the TiO_2 network. The bands at 1055, 1035, and 1010 cm^{-1} are related to vibration modes of the Ti-O-C functional group due to carbonate species linked to the catalytic support [22-24]. No other peaks were observed, due to the CeO_2 and V_2O_5 low content in relation to the TiO_2 amount.

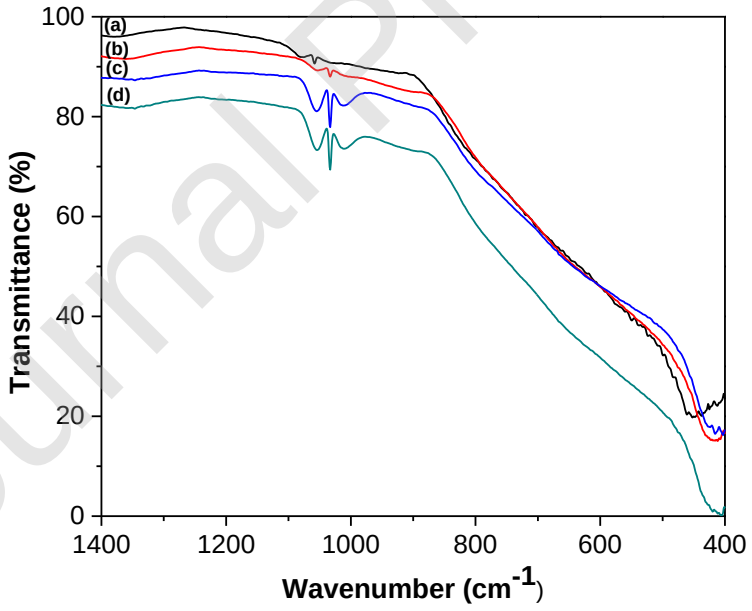

Figure 2. FT-IR spectra of the (a) TiCe, (b) TiCe-3V_2O_5, (c) TiCe-6V_2O_5, and (d) TiCe-10V_2O_5 catalysts.

3.3 Raman spectroscopy

The TiCe and TiCe-V_2O_5 catalysts characterized by Raman spectroscopy show the spectra of Figure 3. All the Raman spectra look very similar. The signals located at 1443, 196, 396, 514, and 639 cm^{-1} are characteristic of the tetragonal anatase phase. No Raman bands corresponding to the rutile phase of TiO_2 were detected. However, the signal close to 460 cm^{-1} corresponds to the CeO_2 cubic phase [25-27]. The spectra in the region of 1000 to 2000 cm^{-1} show vast peaks between 1403 and 1549 cm^{-1}, corresponding to carbon species. In these spectra, characteristic signals of CeO_2 and V_2O_5 were not identified, so another region of the materials was analyzed.

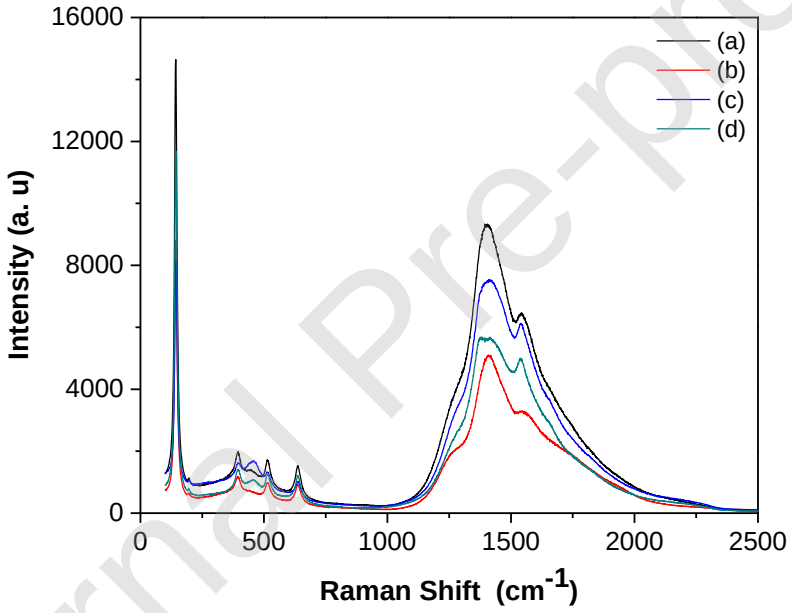

Figure 3. Raman spectra of the (a) TiCe-10V_2O_5, (b) TiCe-6V_2O_5, (c) TiCe-3V_2O_5, and (d) TiCe catalysts.

Figure 4 belongs to the Raman spectrum of the TiCe-V_2O_5 catalysts, where small peaks are observed in the region of 100 to 600 cm^{-1}. The peak located at 461 cm^{-1} is due to CeO_2, while the peaks at 633, 514, and 201 cm^{-1} correspond to the anatase phase of titanium oxide. The peaks at 791 and 913 cm^{-1} correspond to vibrations from V_2O_5, and these peaks are greatly diminished due to the intensity of the peaks of TiO_2 in its anatase phase, and the low amount of V_2O_5 in the catalysts.

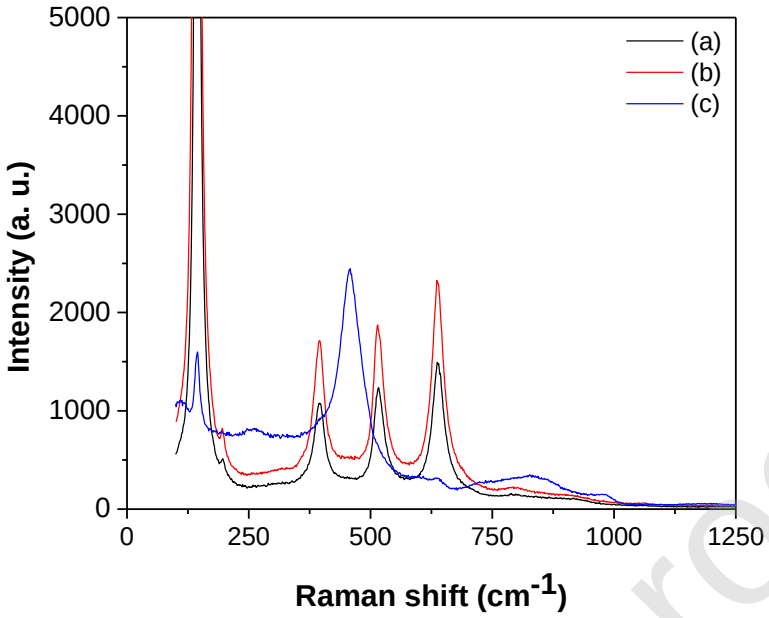

Figure 4. Raman spectra of the different TiCe-V_2O_5 catalysts (a) $3V_2O_5$, (b) $6V_2O_5$, and (c) $10V_2O_5$ respectively.

3.4 X-ray diffraction

Figure 5 displays the X-ray diffraction patterns of the TiCe and TiCe-V_2O_5 catalysts. All diffractograms show very similar peaks. The signals at 2θ = 25, 37, 48, 54, 55, 62,68 71 and 75 degrees characterize the tetragonal anatase phase of titanium oxide (indicated by letter A in Figure 5). Besides, the other two peaks seen at 2θ=28 and 33 degrees are related to the CeO_2 in the cubic phase. The absence of signals from V_2O_5 suggests that the low amount of this compound did not allow the generation of any signal, due to the fact that it was profusely distributed in the material

.

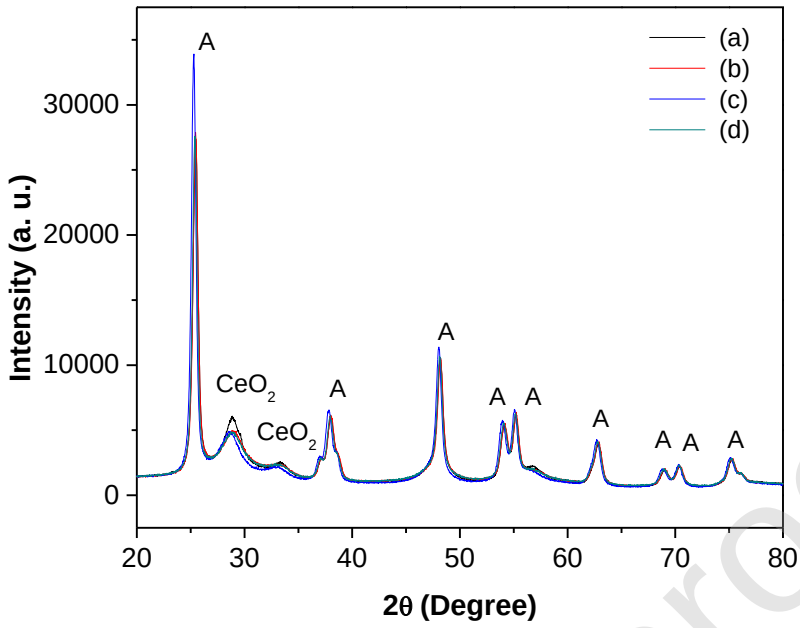

Figure 5. X-ray diffractograms of the (a) TiCe-10V_2O_5, (b) TiCe-6V_2O_5, (c) TiCe-3V_2O_5, and (d) TiCe catalysts. Letter A indicates the anatase phase.

3.5 X-ray photoelectron spectroscopy

The XPS photoemission spectra of the Ti2p exhibits the characteristic peaks between 458-459 eV intervals from Ti2p3/2 (Figure 6). Therefore, it can be inferred that titanium atoms are mainly limited by its highest oxidation state (IV).

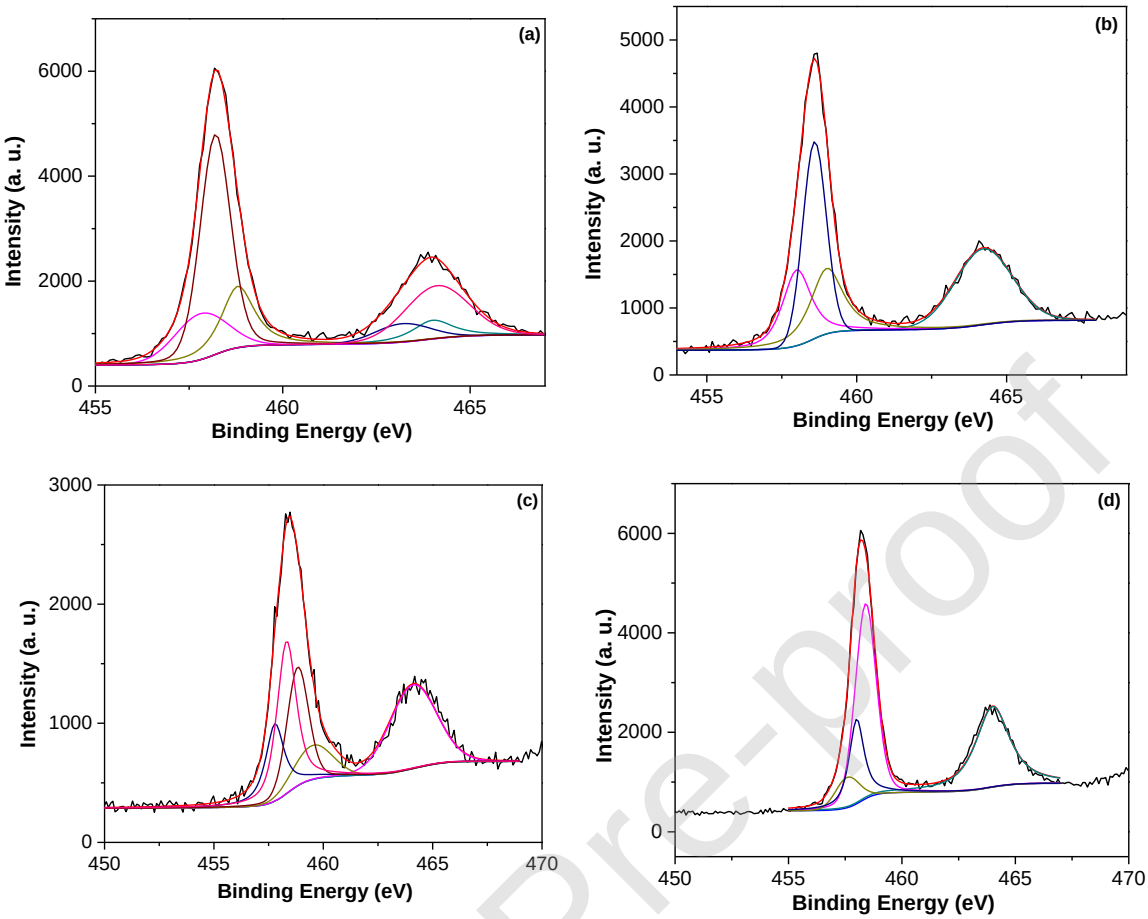

Figure 6. XPS spectra of Ti atom in the catalysts

a) TiCe, b) TiCe-3V_2O_5, c) TiCe-6 V_2O_5, and d) TiCe-10V_2O_5

The TiO_2 shows the Tip3/2 and Tip1/2 binding energies (BE) which correspond to BE of pure TiO_2. The Ti2p1/2 peak appears at 464.2 eV. This value is slightly higher than that reported in the literature (458-459 eV) [11-15]. Sharp and intense peaks indicate that the TiO_2 consists only of Ti^{+4} ions in the lattice. Other signals are observed at 459 eV and 464.7 eV which are related to the doublet of the orbital Ti 2p and are modified when: 1) the crystalline phase of Ti^{4+} is not only one, 2) symmetry and resolution effects occur, due to the passage of energy (CAE) in the acquisition of the spectrum, and 3) the presence of vacancies. The separation of the doublets of Ti2p is fixed for each oxidation state and each crystalline anatase phase of TiO_2. The binding energies of Ti 2p3/2 for the anatase phase is 458.70 eV.

Figure 7 shows peaks in the region centered between peaks 515.6 eV and 517.1 eV for the catalysts; these peaks are ascribed as the vanadium oxidations V^{4+} and V^{5+} respectively. The V^{4+} and V^{5+} pair can transfer electrons to the Ce^{4+} by reducing it. The band at 529.7 eV is the O1s peak corresponding to the oxygen network, while the peak at 531.68 eV corresponds to the oxygen absorbed at the surface [28].

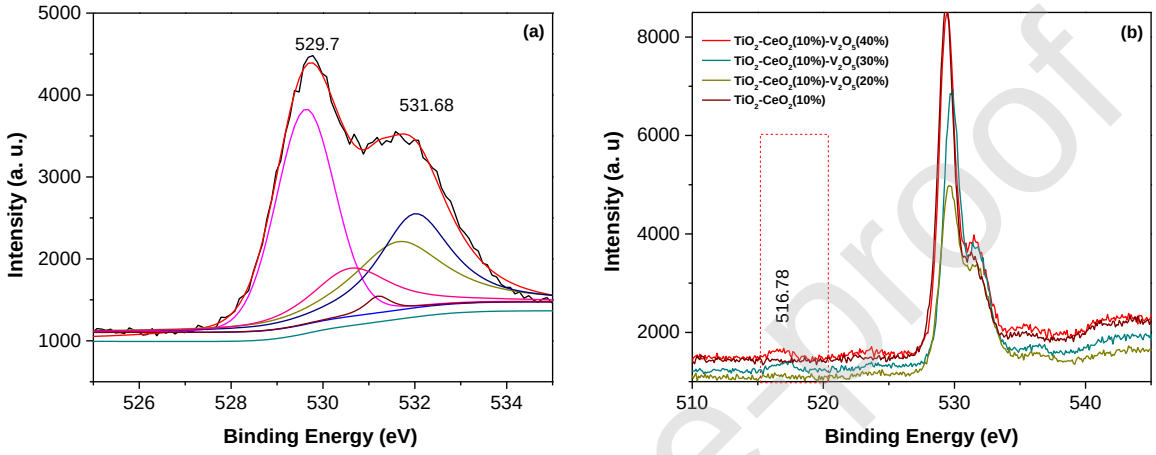

Figure 7. XPS spectra of vanadium in the catalysts a) oxygen in the samples and b) vanadium in all the samples.

The complex spectrum of Ce was decomposed into eight components, which were assigned as is shown in Figure 8. In these figures the Ce^{3+}/Ce^{4+} initial signals are extensive, corresponding to several overlapping signals. The large number of signals in the spectra are due to the electronic structure of the cation and the spin-orbit coupling of cerium. To carry out the experiment, it was necessary to excite electrons from layer d to move to layer f of valence, thus producing a series of possible electronic transitions. The sub-bands designated u' and v' represent the initial electronic state $3d^{10}4f^{1}$ corresponding to Ce^{3+}, and the labels u, u', u", v, v', and v" represent the initial electronic state corresponding to Ce^{4+}. The peaks labeled as u are due to spin-orbital $3d^{3/2}$ states, and those that are marked as v correspond to state $3d^{5/2}$. The doublet of u'"/v'" is due to the photoemission of Ce (IV)-O_2. The peaks labeled as u/v and u"/v" radically change their characteristics and they are the result of the transfer of one or two electrons from a full orbital of the O 2p to an empty orbital of the Ce 4f. The bands designated as u'/v' are the result of the photoemission of Ce (III) cations

which denotes a mixture of the oxidation states of Ce^{3+}/Ce^{4+} and an increase of the numerous peaks indicating that the surface of the sample is not completely oxidized. An additional peak centered at 880.9 eV is the result of the transfer of an electron from the O 2p orbital to the Ce 4f orbital during the photoemission of Ce^{3+} cations [29].

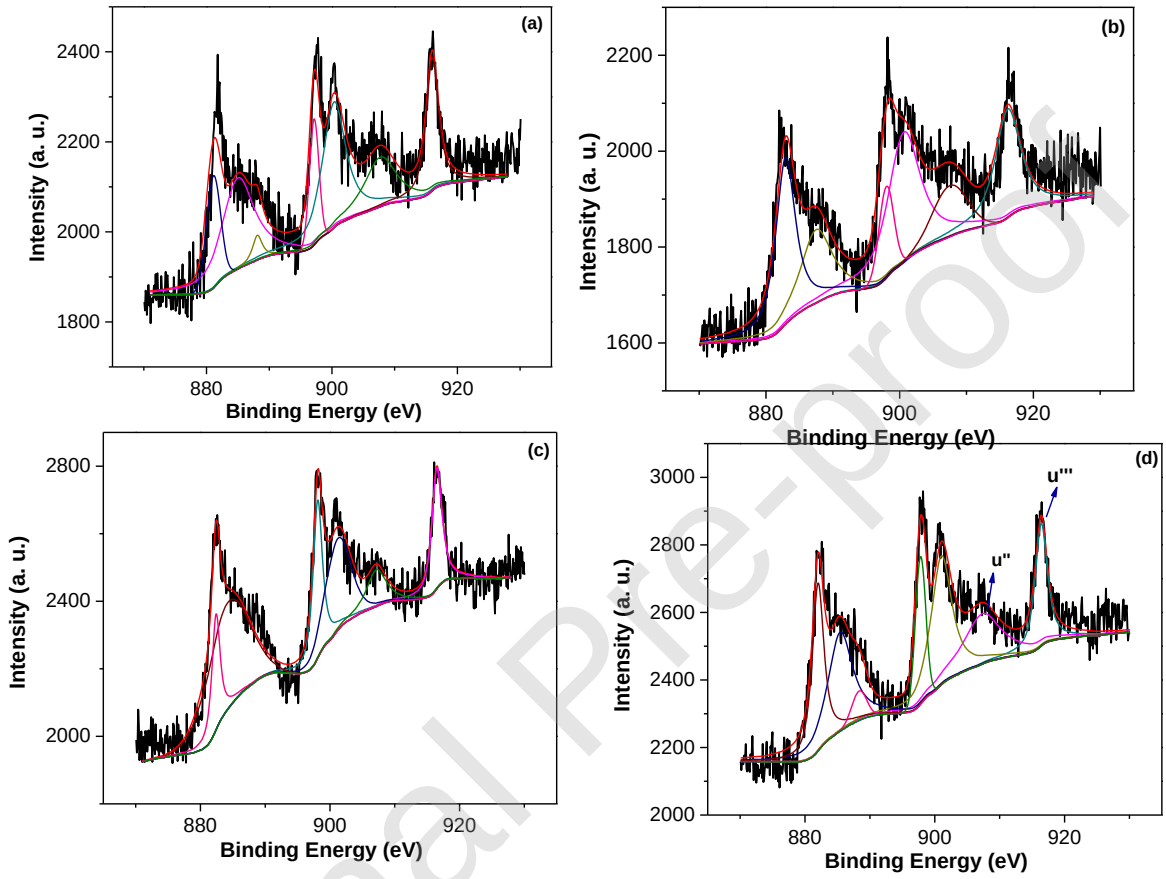

Figure 8. XPS spectra of Ce atoms in the catalysts (a)TiCe, b) TiCe-3V_2O_5, c) TiCe-6V_2O_5, and (d) TiCe-10V_2O_5.

3.6 Band gap energy values determination

The band gap (Eg) values of the catalysts, which were determined by the XPS measurements [21], are reported in Figure 9 and Table 3**,** respectively.

Our interest in obtaining the TiCe-V_2O_5 catalysts lies in the fact that they show high conductivity and transparency in the visible region of the electromagnetic spectrum. These features are motivating since many solids have forbidden energy bands (1-5.0 eV), higher

than the energy interval of the visible spectrum (1.6-3.1 eV), thus hindering light absorption. Besides, these catalysts are chemically stable under atmospheric conditions, do not undergo oxidation, and their properties can be manipulated by doping with other cations or by controlling the concentration of oxygen vacancies.

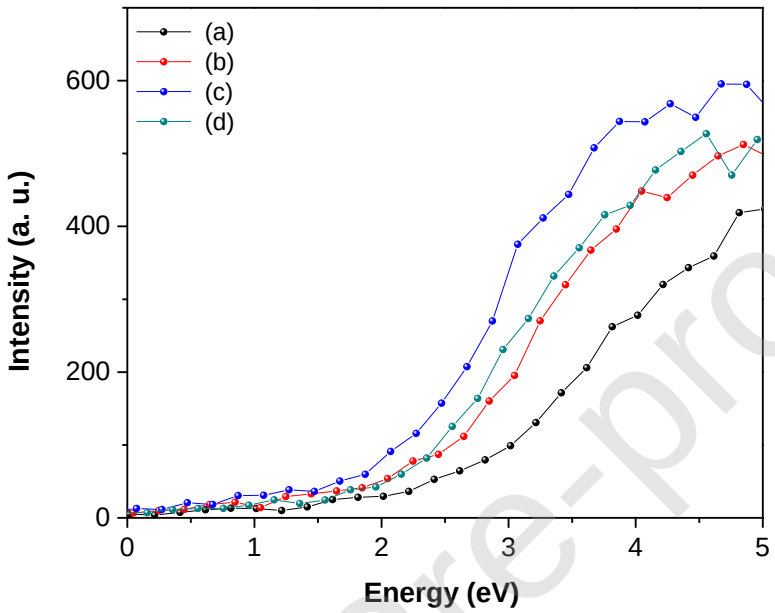

Figure 9. Valence band spectra and d-band center energies calculated for: (a) TiCe-10V_2O_5, (b) TiCe-6V_2O_5, (c) TiCe-3V_2O_5, and (d) TiCe catalysts.

Table 3. Band energy values of the different catalysts.

Sample	Band energy (eV)
TiCe	2.1
TiCe-3V_2O_5	2.0
TiCe-6V_2O_5	1.5

TiCe-10V_2O_5	1.8

The band energy is undoubtedly essential for electronic mobility, the closer the gap between the valence band and the conduction band, the higher the electronic movement. The combination of CeO_2 and TiO_2 lowers the band gap values of both individual oxides from around 3-3.6 eV to 2.1 eV. In Table 3, it can be seen that the band energy decreases as the percentage of vanadium oxide increases, moving towards the visible region.

The band energy is lower in materials containing vanadium oxide because when incorporated into the TiCe matrix, defects in the structure are generated, causing vacancies [30]. As a result, the prohibited band decreases, and the electron-hollow pair movement increases, increasing the formation of OH ° radicals, especially when hydrogen peroxide is added to the reaction medium. The creation of OH radicals is essential because they are potent oxidizing agents and an excellent source of free radicals, a necessary factor in oxidation reactions.

3.7 Catalytic reaction tests

It is difficult to establish a criterion to quantify and to properly identify reaction products. However, qualitative techniques granted us valuable information. In this work, the reaction products were identified by FTIR and ^{13}C-NMR based on the previous methodology reported by Manríquez et. al [31], and then they were quantified by gas chromatography. The reaction products obtained by chemical oxidation reaction and analyzed by infrared spectroscopy are shown in Figure 10a. It is possible to observe that as the vanadium content increases, the OHs band increases. This band may be due to the formation of the expected alcohols (1-phenylethanol and 2-phenylethanol). However, benzaldehyde was also identified by the -CH_3 (methyl ester) band which appeared at 2951 cm^{-1}; the C=O group became visible at 1725 cm^{-1}, the asymmetric scissors deformation of -CH_2 band around 1442 cm^{-1}, the stretching of C-O band around 1142 cm^{-1}, the C-O-C band at 985 cm^{-1}, and the skeleton CH_2 band at 750 cm^{-1}. All infrared bands show a substantial intensity incremented by the catalyst with the highest amount of V_2O_5.

Figure 10b corresponds to the infrared spectra of the reaction products obtained by the photocatalytic process. The signals also correspond to the alcohols and the benzaldehyde previously identified. The only difference is that the OH band from the alcohols had the same intensity for all catalysts tested. This result suggests that the catalytic conversion was faster by irradiation with ultraviolet light. This fact may be due to the fact that the three oxides in the catalysts absorb UV radiation, thus accelerating the electronic mobility and the reaction velocity too.

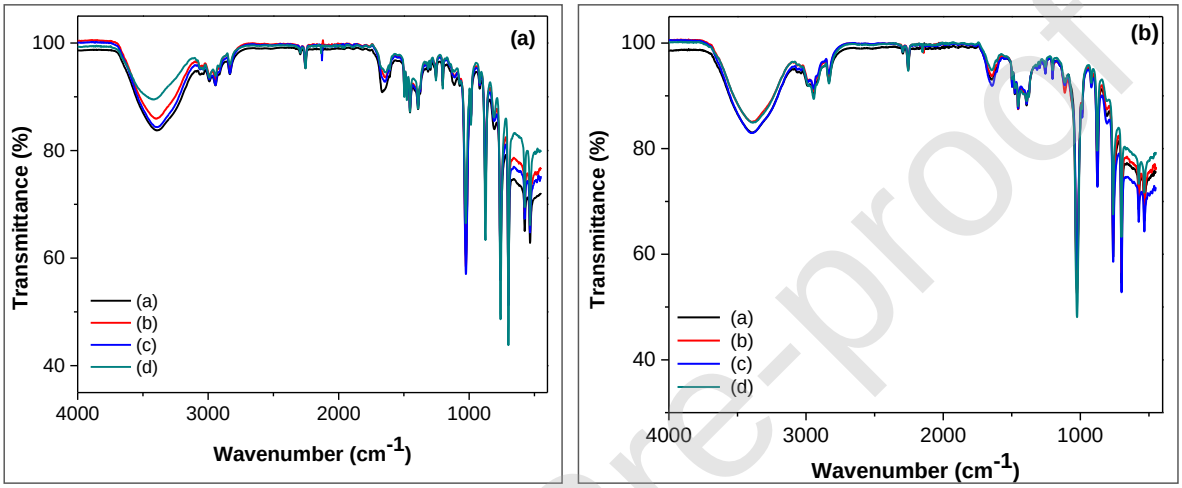

Figure 10. (a) Infrared spectra of reaction products obtained by chemical oxidation reaction using the (a) TiCe-10V_2O_5, (b) TiCe-6V_2O_5, (c) TiCe-3V_2O_5, (d) TiCe catalyst. **(b)** Infrared spectra of reaction products obtained by Photochemical reaction using (a) TiCe-10V_2O_5, (b) TiCe-6V_2O_5, (c) TiCe-3V_2O_5, and (d) TiCe catalysts.

The ^{13}C NMR spectra of the reaction products obtained by chemical oxidation displayed in Figure 11a show the characteristic peaks of 2-phenylethanol and 1-phenylethanol as a mixture, while the characteristic signals of benzaldehyde were not identified, maybe because the low amount obtained of this compound. The signals identified by ^{13}C NMR at δ= 134.86 (C-1'), 125.09 (C-2' y 6'), 124.49 (C-3' y 5'), 122.34 (C-4'), and 128,36 (C-4'), 126,51 (C-2' and 6'), 75,13 (C-2), 53.3(C-1') ppm correspond to 2-phenylethanol. The signals between 50 and 60 ppm observed as multiplets correspond to the C-OH group from the two alcohols registering the same signals. The ^{13}C-NMR spectra revealed that the compounds structure matches with the 1-phenylethanol and 2-phenylethanol structures, while 2-phenylethanol was the most significant product when the reaction was carried out under ultraviolet radiation. The intensity of the peaks varies according to the catalyst used; and the most intense peaks appeared with the catalyst containing the higher V_2O_5 amount.

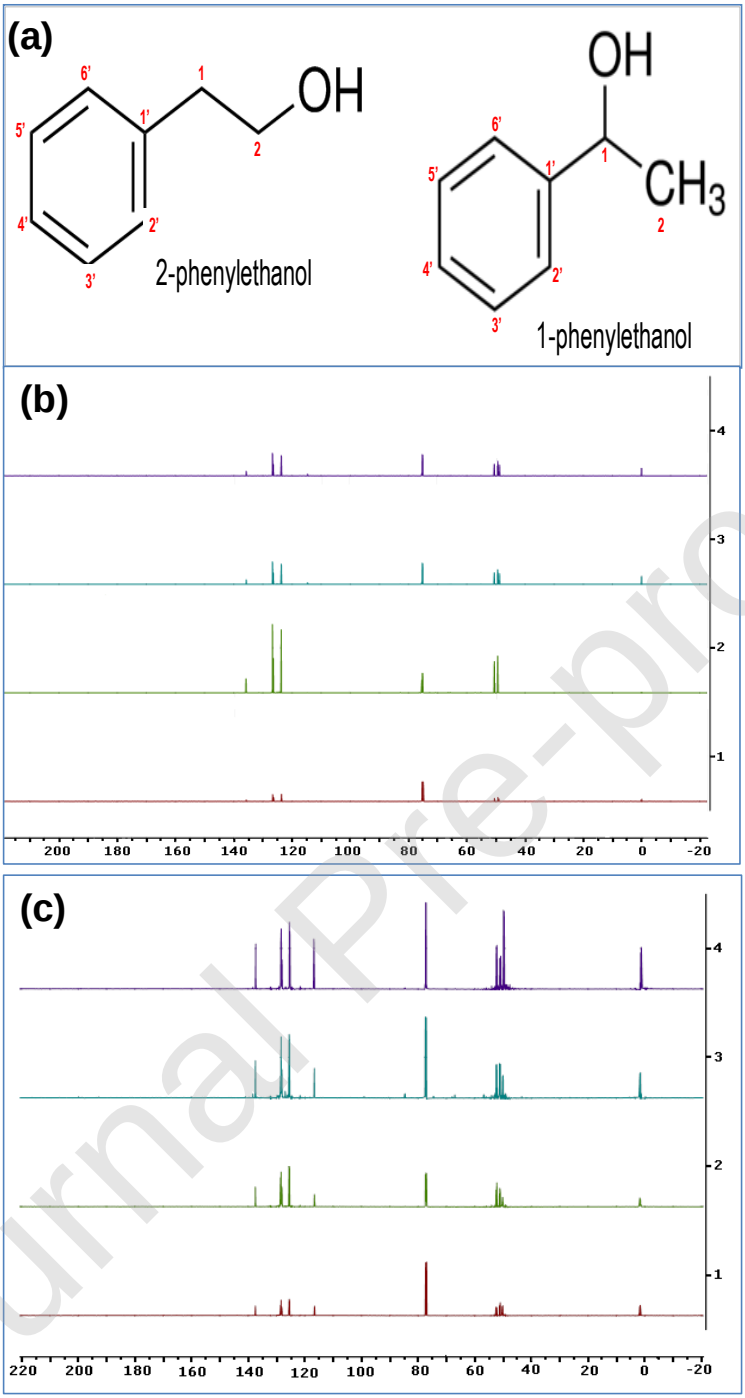

Figure 11. (a) Chemical structure of 2-phenylethanol and 1-phenylethanol, ^{13}C-MNR spectra of the reaction products by (b) chemical oxidation using the (purple) TiCe-10V_2O_5, (cyan) TiCe-6V_2O_5, (green) TiCe-3V_2O_5 and (coffee) TiCe catalysts, and (c) photochemical oxidation reaction using the TiCe-10V_2O_5 (purple), TiCe-6V_2O_5 (cyan), TiCe-3V_2O_5 (green) and TiCe (coffee) catalysts.

3.8 Conversion and catalytic selectivity

Figure 12 shows the conversion via chemical and photochemical routes for each catalyst. The best conversions were obtained by the photochemical process, and the catalytic conversion rose when the vanadium oxide amount increased.

Figure 13 shows that the dominant reaction products (by both methods) were 1-phenylethanol and 2-phenylethanol; however, a low amount of benzaldehyde was identified when the catalytic support was tested without light irradiation (Figure 13a). The photochemical process yields better selectivity to 2-phenylethanol. The 1-phenylethanol and benzaldehyde production decreases as V_2O_5 increases due to its better selectivity to the 2- phenylethanol. Figure 13b shows that the selectivity to 2-phenylethanol is almost 100% in the catalyst that has the greater amount of vanadium oxide, and that traces of benzaldehyde can be observed. However, the selectivity increases to 2-phenylethanol when the reaction is irradiated with ultraviolet light.

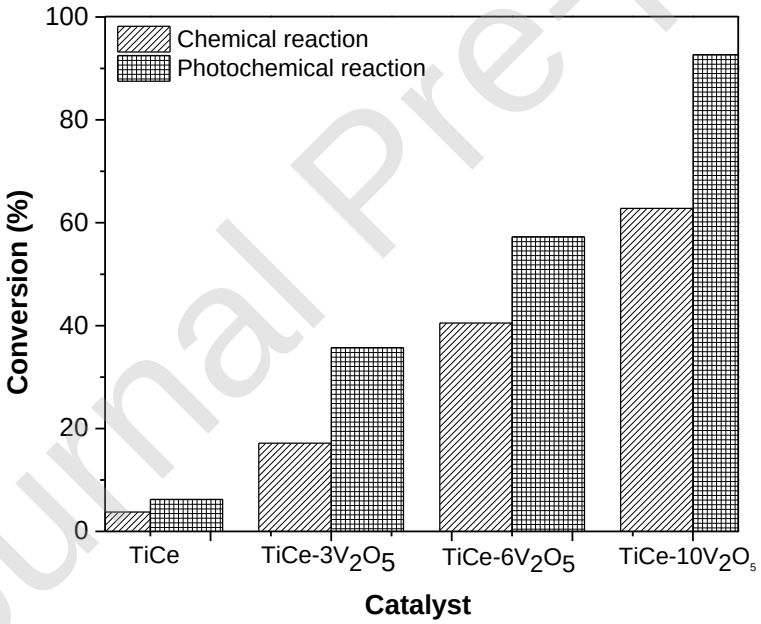

Figure 12. Conversion catalytic of styrene oxide via a chemical and photochemical process using TiCe-V_2O_5 catalysts.

The oxidation reaction occurs more slowly without ultraviolet light irradiation leading to a slower reaction path and allowing the possibility of the mixture of alcohols and phenylacetaldehyde formation. This latter is formed by a nucleophilic attack of H_2O_2 on

styrene oxide through a styrene hydroxy peroxide intermediate, as a result of direct oxidation. However, in both of the employed methods the production of phenylacetaldehyde was minimal [32].

In the case of alcohol production, vanadium (V) reacts with H_2O_2 to form an oxometal route in oxidation to alcohol. The simple monovanadate VO_3 efficiently catalyzes oxidations, and it has been shown that the mechanism of this process involves the formation of HO• and HOO • radicals [33]. The first highly reactive radical extracts hydrogen from alcohol to supply the radical RO•, which when reacting with O_2 produces the corresponding alkyl hydroperoxide, ROO •. It is not a very stable species and can easily be transformed into alcohol.

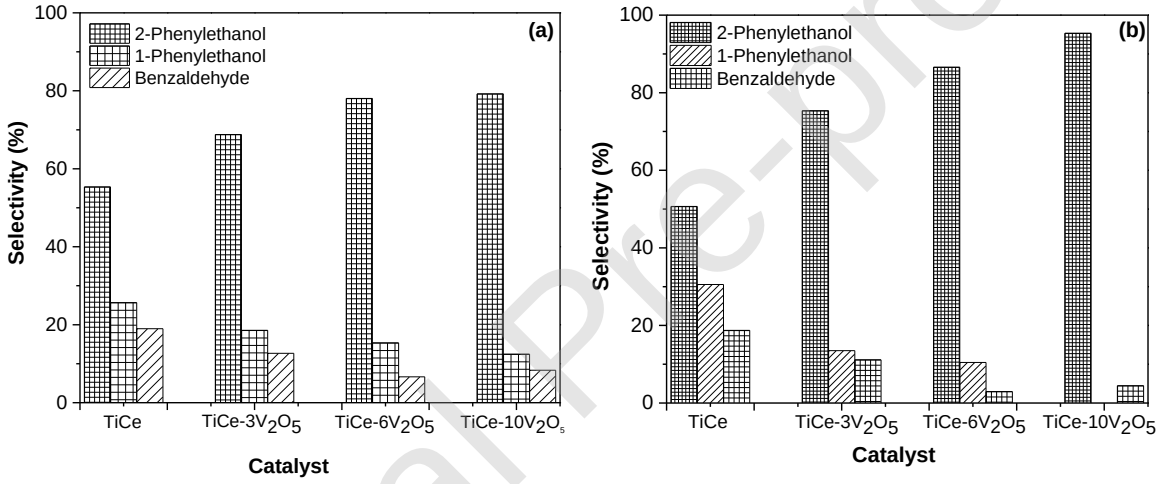

Figure 13. Selectivity catalytic of styrene oxide via (a) chemical and (b) photochemical process using TiCe-V_2O_5 catalysts.

However, it becomes more selective under irradiation. It is remarkable that this type of reaction reported by other authors starts from styrene, passing to epoxide and from there to alcohol and, subsequently, to the corresponding aldehyde [34, 35]. In this work, the irradiation modifies the selectivity. It should be noted that to obtain 2-phenylethanol many reactions are carried out by styrene oxide hydrogenation reactions using metals such as Pt and Pd as hydrogenation catalysts [34-36], which turn out to be expensive, hence the importance of this oxidation method to obtain similar products.

4. Conclusions

1. TiCe-V_2O_5 catalysts were successfully obtained by the co-precipitation method.
2. No effect of the content of the vanadium oxide on the textural properties of the catalysts was observed. The surface area, pore volume, and diameter values were similar for all catalysts.
3. The bandgap energy value for the combined TiO_2-CeO_2 catalytic support decreases from around 3-3.6 to 2.1 eV.
4. The catalytic activity increases as the V_2O_5 amount rises, and with ultraviolet light radiation.
5. The most significant reaction products were 2-phenylethanol and 1- phenylethanol; however, a small amount of phenylacetaldehyde was identified and quantified.
6. The selectivity to 2-phenylethanol increased with the ultraviolet light irradiation.
7. 2-Phenylethanol is mainly obtained from styrene oxide hydrogenation reactions using, as hydrogenation catalysts, expensive metals such as Pt and Pd. Hence the importance of the method reported in this work that consists of the oxidation process of styrene oxide using more selective and inexpensive catalysts to obtain the same products obtained here.

Author Statement

Ma. Elena Manríquez: Conceptualization, Investigation, Resources, **Martín Trejo Valdez**: Formal analysis, **Andrea Sánchez Pliego**: Methodology, **Laura V. Castro**: Formal analysis, **Emma Ortiz-Islas**: Writing-Original Draft, Supervision, Writing-Review & Editing.

A**cknowledgment:**

This work was supported by National Polytechnic Institute through projects 20201448 and 20200423

References

[1] C. Ragupathi, J.J. Vijaya, R.T. Kumar, L.J. Kennedy, Selective liquid phase oxidation of benzyl alcohol catalyzed by copper aluminate nanostructures, J. Mol. Struct. 1079 (2015) 182-188. https://doi.org/10.1016/j.molstruc.2014.09.045

[2] O.A. Kholdeeva, N.V. Maksimchuk, G.M. Maksimov, Polyoxometalate-based heterogeneous catalysts for liquid phase selective oxidations: Comparison of different strategies, Catal. Today. 157 (2010) 107-113. https://doi.org/10.1016/j.cattod.2009.12.016.

[3] M.G. Clerici, O.A. Kholdeeva, Liquid Phase Oxidation Via Heterogeneous Catalysis. Organic Synthesis and Industrial Applications, first ed., John Wiley & Sons, Incorporated, New Jersy, 2013.

[4] S. Rautiainen, O. Simakova, H. Guo, A. R. Leino, K. Kordás, D. Murzin, M. Leskelä, T. Repo, Solvent controlled catalysis: Synthesis of aldehyde, acid or ester by selective oxidation of benzyl alcohol with gold nanoparticles on alumina, Appl. Catal., A. 485 (2014) 202-206. https://doi.org/10.1016/j.apcata.2014.08.003

[5] Y. Shin, S. Sharma, N.K. Mishra, S. Han, J. Park, H. Oh, J. Ha, H. Yoo, Y.H. Jung, I.S. Kim, Direct and Site-Selective Palladium-Catalyzed C-7 Acylation of Indolines with Aldehydes, Adv. Synth. Catal. 357 (2015) 594-600. https://doi.org/10.1021/ol400206k

[6] K. Negi, M. Kumar, G. Singh, S. Chauhan, M.S. Chauhan, Nanostructured CeO_2 for selective-sensing and smart photocatalytic applications, Ceram. Int. 44 (2018) 15281-15289. https://doi.org/10.1016/j.ceramint.2018.05.172

[7] Z. Liu, S. Guo, C. Hong, Z. Xia, Synthesis and photocatalytic properties of CeO_2 nanocubes, J Mater Sci: Mater. Electron. 27 (2016) 2146-2150. 10.1007/s10854-015-4004-1

[8] F. Chen, Y. Cao, D. Jia, Preparation and photocatalytic property of CeO_2 lamellar Appl. Surf. Sci. 257 (2011) 9226-9231. 10.1016/j.apsusc.2011.06.009

[9] P. Min, S. Zhang, Y. Xu, R. Appl. Surf. Sci. 448 (2018) 435-443. 10.1016/j.apsusc.2018.04.103

[10] H. Imagawa, A. Suda, K. Yamamura, S. Sun, J. Phys. Chem. C. 115 (2011) 1740-1745. https://doi.org/10.1021/jp109878j

[11] H. Boucard, M. Watanabe, S. Takami, E. Weiss-Hortala, R. Barna, T. Adschiri, Enhanced oxygen storage capacity of CeO_2 with doping-induced unstable crystal structure, J. Supercrit. Fluid. 105 (2015) 66-76. https://hal.archives-ouvertes.fr/hal-01611094

[12] H.T. Kwon, M.P. Bukhovko, S. Mahamulkar, T. Sulmonetti, B. Min, Q. Almas, Sol-Gel Derived CeO_2/α-Al_2O_3 Bilayer Thin Film as an Anti-Coking Barrier and Its Catalytic Coke Oxidation Performance, AIChE J. 64 (2018) 4019-4026. 10.1002/aic.16383

[13] H.L. Koh, H.K. Park, Characterization of MoO_3-V_2O_5/Al_2O_3 catalysts for selective catalytic reduction of NO by NH_3, J. Ind. Eng. Chem. 19 (2013) 73-79. 10.3390/catal9060527

[14] N.Y. Topsøe, Science mechanism of the Selective Catalytic Reduction of Nitric Oxide by Ammonia Elucidated by in Situ On-Line Fourier Transform Infrared Spectroscopy, Science. 265 (1994) 1217-1219. http://dx.doi.org/10.1126/science.265.5176.1217

[15] V.C. Anitha, A.N. Banerjee, S.W. Joo, Recent developments in TiO_2 as n- and p-type transparent semiconductors: synthesis, modification, properties, and energyrelated applications, J. Mater. Sci. 50 (2015) 7495-7536. 10.1007/s10853-015-9303-7

[16] C. Lamsal, N.M. Ravindra, Optical properties of vanadium oxides-an analysis, J. Mater. Sci. 48 (2013) 6341-6351. 10.1007/s10853-013-7433-3

[17] V. Sydorchuk, O. Makota, S. Khalameida, L. Bulgakova, J. Skubiszewska-Zie¸ba, R. Leboda, V. Zazhigalov, Physical-chemical and catalytic properties of deposited MoO_3 and V_2O_5, J. Therm. Anal. Calorim. 108 (2012) 1001-1008. 10.1007/s10973-011-1895-9

[18] X. Zhang, C. Li, L. Zhao, J. Zhang, G. Zeng, Y. Xie, M. Yu, Simultaneous removal of elemental mercury and NO from flue gas by V_2O_5-CeO_2/TiO_2 catalysts.

Appl. Surf. Sci. 347 (2015) 392-400. http://dx.doi.org/10.1016/j.apsusc.2015.04.039

[19] Y. Yang, W. Xu, J. Wang, T. Zhu, New insight into simultaneous removal of NO and Hg0 on CeO_2-modified V_2O_5/TiO_2 catalyst: A new modification strategy. Fuel 249 (2019) 178-187. https://doi.org/10.1016/j.fuel.2019.03.103

[20] J. Arfaoui, A. Ghorbel, C. Pettito, G. Delahay, Novel V_2O_5- CeO_2-TiO_2-SO_4^{2-} nanostructured aerogel catalyst for the low temperature selective catalytic reduction of NO by NH_3 in excess of O_2. Appl. Catal., B. 224 (2018) 264-275. http://dx.doi.org/10.1016/j.apcatb.2017.10.059

[21] E.A. Kraut, R.W. Grant, J. R. Waldrop, S. P. Kowalczyk. Semiconductor core-level to valence-band maximum binding-energy differences. Precise determination by x-ray photoelectron spectroscopy, Phys. Rev. B 28 (1983) 1965-1977.

[22] J. Lin, J. C. Yu, J. Photochem. An investigation on photocatalytic activities of mixed TiO_2-rare earth oxides for the oxidation of acetone in air, Photobiol. A. 116 (1998) 63-67. https://doi.org/10.1016/S1010-6030(98)00289-5

[23] Y. Jiang, X. Wang, Z. Xing, C. Bao, G. Liang, Preparation and characterization of CeO_2-MoO_3/TiO_2 catalysts for selective catalytic reduction of NO with NH_3, Aerosol. Air. Qual. Res. 17 (2017) 2726-2734. 10.4209/aaqr.2016.08.0352

[24] L.A. De Faria, S. Trasatti, The point of zero charge of CeO_2, J. Colloid. Interface Sci. 167 (1994) 352-357. https://doi.org/10.1006/jcis.1994.1370

[25] Y. Jiang, Z. Xing, X. Wang, S. Huang, Q. Liu, J.Yang, MoO_3 modified CeO_2/TiO_2 catalyst prepared by a single step sol-gel method for selective catalytic reduction of NO with NH_3, J. Ind. Eng. Chem. 29 (2015) 43- 47. https://doi.org/10.1016/j.jiec.2015.04.023

[26] M.A. Banares, I.E. Wachs, Molecular structures of supported metal oxide catalysts under different environments, J. Raman Spectrosc. 33 (2002) 359-380. https://doi.org/10.1002/jrs.866.

[27] B. Olthof, A. Khodakov A.T. Bell, E. Iglesia, Effects of Support Composition and Pretreatment Conditions *on* the Structure of Vanadia Dispersed *on*

SiO_2, Al_2O_3, J. Phys. Chem. B. 104 (2000) 1516-1528. https://doi.org/10.1021/jp9921248

[28] T. Hirata, A. Watanabe, Raman and Infrared Spectroscopic Study of Ce1-xMxVO_4-0.5 x (M= Pb, Sr, and Ca) and Ce1-xBixVO_4 Solid Solutions, J. Solid. State. Chem. 158 (2001) 254-259. https://doi.org/10.1006/jssc.2001.9101

[29] S. Point, T. Minea, B. Bouchet-Fabre, A. Granier, G. Turban, XPS and NEXAFS characterisation of plasma deposited vertically aligned N-doped MWCNT, Diam. Relat. Mater. 14 (2005) 891-895. https://doi.org/10.1016/j.diamond.2004.10.011

[30] B.M. Reddy, A. Khan, Y. Yamada, T. Kobayashi, Structural Characterization of CeO_2-TiO_2 and V_2O_5/CeO_2-TiO_2 Catalysts by Raman and XPS Techniques, J. Phys. Chem. B. 107 (2003) 5162-5167. https://doi.org/10.1021/jp0344601

[31] M. E. Manríquez, G. Morales-Mendoza, J. Alamilla, U. Trejo, R. Gómez, E. Ortiz-Islas. Photocatalytic oxidative esterification of benzaldehyde by V2O5–ZnO catalysts. Reac. Kinet. Mech. Cat. 122 (2017) 1281-1296. DOI 10.1007/s11144-017-1262-3

[32] C. Chiappe, A. Sanzone, P.J. Dyson, Styrene oxidation by hydrogen peroxide in ionic liquids: The role of the solvent on the competition between two Pd-catalyzed processes, oxidation and dimerization. Green Chem. 13 (2011) 1437-1441. doi: 10.1039/C0GC00945H

[33] K. Hermann, M. Witko, R. Druzinic, R. Tokarz, Oxygen vacancies at oxide surfaces: abinitio density functional theory studies on vanadium pentoxide, Appl. Phys. A Mater. Sci. Process. 72 (2001) 429-442. 10.1007/s003390100756

[34] I. Kirm, F. Medina, X. Rodriguez, Y. Cesteros, P. Salagre, J.E. Sueiras, Preparation of 2-phenylethanol by catalytic selective hydrogenation of styrene oxide using palladium catalysts. J. Mol. Catal. A Chem. 239 (2005) 215-221. doi:10.1016/j.molcata.2005.06.032

[35] M. Ghafouri, M. Moghadam, K. Mehrani, A. Daneshvar, Supported ruthenium hydride catalysts for directconversion of alcohols to carboxylic acids

using styrene oxide as oxidant. Appl. Organometal. Chem. 32 (2018) 1-6. DOI: 10.1002/aoc.4048

[36] I. Kirm, F. Medina, J.E. Sueiras, P. Salagre, Y. Cesteros, Hydrogenation of styrene oxide in the presence of supported platinum catalysts to produce 2-phenylethanol. J. Mol. Catal. A Chem. 261 (2007) 98-103. doi:10.1016/j.molcata.2006.07.043